Applied Materials Today 26 (2022) 101280

Contents lists available at ScienceDirect

Applied Materials Today

journal homepage: www.elsevier.com/locate/apmt

Surface engineering of plasmonic gold nanoisland platforms for high-sensitivity refractometric biosensing applications

Youngkyu Hwang[a,b], Abdul Rahim Ferhan[b], Bo Kyeong Yoon[a,c], Tun Naw Sut[a,b], Won-Yong Jeon[a], Dong Jun Koo[a], Joshua A. Jackman[a,*], Nam-Joon Cho[b,*]

[a] School of Chemical Engineering and Biomedical Institute for Convergence at SKKU (BICS), Sungkyunkwan University, Suwon 16419, Republic of Korea
[b] School of Materials Science and Engineering, Nanyang Technological University, Singapore 639798, Singapore
[c] School of Healthcare and Biomedical Engineering, Chonnam National University, Yeosu 59626, Republic of Korea

ARTICLE INFO

Article history:
Received 13 September 2021
Revised 3 November 2021
Accepted 15 November 2021
Available online 25 November 2021

Keywords:
Nanoplasmonics
Nanoisland
Nanofabrication
Biosensing
Surface functionalization

ABSTRACT

Plasmonic chips comprising gold nanoisland structures that are fabricated by solution-phase seeding, have demonstrated excellent promise as high-sensitivity substrates for molecular detection and medical diagnostic applications. Even so, there still remains an outstanding need to examine the potential utility of these plasmonic chips for label-free refractometric biosensing and to understand how nanostructure design principles affect measurement sensitivity. Herein, we developed a thiol-based surface functionalization strategy to fabricate gold nanoislands on a functionalized glass surface with improved fractional surface coverages and inter-island gap distances of 80–85% and 5–10 nm, respectively, as compared to values of 50–65% and 15–20 nm for gold nanoislands on bare glass substrates. By tuning the gap distance, it was possible to adjust the bulk refractive index sensitivity of the measurement signal from ~99 nm per refractive index unit (nm/RIU) for gold nanoislands on a non-functionalized glass surface to ~180 nm/RIU for gold nanoislands on a functionalized glass surface. The nanoplasmonic biosensing capabilities of the latter plasmonic chip were further investigated and demonstrated larger measurement responses for detecting bovine serum albumin (BSA) protein adsorption compared to other types of plasmonic gold nanostructures. It was also possible to detect antigen-antibody interactions related to coronavirus disease-2019 (COVID-19), especially binding events that occurred near the sensor surface. These findings demonstrate the broad application possibilities of gold nanoisland platforms for refractometric biosensing and emphasize the importance of finetuning nanostructure dimensions to optimize sensing performance.

1. Introduction

The interaction of light with gold nanostructures such as nanoparticles [1,2], nanoislands [3,4], and nanodisks [5,6] can give rise to unique optical properties that are distinct from those of bulk gold [7–9]. In particular, light-induced coherent oscillation of conduction-band electrons near the nanostructure surface can generate a plasmon-enhanced electromagnetic field that surrounds the gold nanostructure and is sensitive to changes in the local refractive index, *e.g.*, when a biomolecule adsorbs onto the surface [10]. The corresponding optical properties depend on the nanostructure geometry and trackable spectral features are typically found in the visible–near–infrared wavelength range. As such, there is broad interest in fabricating nanostructured films for various nanoplasmonic sensing strategies involving the localized surface plasmon resonance (LSPR) [11–14], surface-enhanced Raman spectroscopy (SERS) [15–19], and plasmon-enhanced fluorescence emission measurement concepts [20].

Among various options, plasmonic gold nanoisland films consisting of percolated networks of inhomogenous nanostructures, have received extensive attention for molecular detection applications [21,22]. While the basic measurement principles have been validated in the detection context, there are ongoing efforts to improve gold nanoisland fabrication in terms of factors like homogeneity, reproducibility, and sensing performance. Currently, there are two main strategies to fabricate nanoisland films on solid supports as opposed to physical deposition of already fabricated nanostructures: (1) gold sputtering or evaporation in vacuum, followed by thermal annealing; and (2) solution-phase seeding directly on the solid support [4,21,23–25]. The sputtering/evaporation strategy is widely used due to its high yield and lithography-free process, however, it typically results in significant

* Corresponding authors.
E-mail addresses: jjackman@skku.edu (J.A. Jackman), njcho@ntu.edu.sg (N.-J. Cho).

https://doi.org/10.1016/j.apmt.2021.101280
2352-9407/

variance in nanoisland size that encumbers measurement readouts and weak nanoisland attachment to the solid support impacts stability [3,13,26–28]. On the other hand, solution-phase seeding is more versatile and, with appropriate control of reaction conditions, can yield consistent film morphology across the substrate [4,21,29–31]. It has been extensively used to fabricate gold nanoisland films on bare glass substrates for SERS and plasmon-enhanced fluorescence enhancement applications, while there remains an outstanding need to further explore their utility for refractometric biosensing applications. Within this scope, it would be advantageous to understand how surface functionalization methods could be employed to further improve the nanoisland fabrication process and potentially gain control over key parameters such as inter-island gap distance.

Towards this goal, herein, we report the development of a thiol-based surface functionalization strategy that improves gold nanoisland fabrication by virtue of improving surface adhesion, increasing surface coverage, and decreasing gap distance compared to gold nanoislands fabricated on a bare glass surface. Complementing the surface functionalization strategy, we controlled the extent of nanoisland growth by adjusting the number of growth cycles. The combination of thiol anchoring and growth control enabled us to optimize the inter-island gap distance, which maximized overlap of plasmon-enhanced electromagnetic waves and improved nanoplasmonic biosensing in various application contexts. While gold nanoisland platforms have been fabricated on bare glass surfaces in previous studies, to our knowledge, this is the first attempt utilizing functionalized glass surfaces that enable more robust attachment of gold seeds *via* gold-thiol bonding and greater control over surface morphology, including gap size tuning. Accordingly, our work demonstrates an improved fabrication strategy to produce high-performance gold nanoisland platforms for refractometric biosensing while comprehensively elucidating how fine control of nanoisland surface morphology can modulate surface sensitivity that is applicable to a wide range of material science applications.

2. Materials and methods

2.1. Nanoisland fabrication

Glass slides (Fisherbrand™ Superfrost™ Plus, Thermo Fisher Scientific, Waltham, MA) were used as the substrates and were cleaned sequentially with deionized water (MilliporeSigma, Burlington, MA) followed by acetone incubation with 5 min bath sonication. After drying the samples on a heater plate at 120 °C for 1 min, oxygen plasma treatment (O_2, 99.995%, 10 sccm, 50 W, Daesung Industrial gases Co., Ltd, Seoul, Republic of Korea) was performed for 1 min by using the CUTE-1MPR machine (Femto Science Inc., Hwaseong, Republic of Korea). The samples were then placed in a vacuum chamber with 100 µL of (3-mercaptopropyl)trimethoxysilane (MPTMS) (95%, CAS No.: 4420–74-0, MilliporeSigma) under vacuum condition for 3 h to produce MPTMS-functionalized glass surfaces, resulting in thiol groups on the glass surface. Bare and MPTMS-functionalized glass surfaces were incubated in 200 mL of 5 mM chloroauric acid ($HAuCl_4$, CAS No.: 27,988–77–8, 99.999%, MilliporeSigma) solution and 4 mL of ammonium hydroxide (NH_4OH, 28%, CAS No.: 1336–21–6, MilliporeSigma) was added dropwise under stirring for 1 min, followed by deionized water washing. After incubating the samples in 1 mM sodium tetrahydridoborate ($NaBH_4$, CAS No.: 16,940–66–2, MilliporeSigma) solution for 1 min followed by deionized water washing, 2 or 3 growth cycles were performed depending on the sample and consisted of incubating the substrate in 1500 µM $HAuCl_4$ and 1500 µM hydroxylamine (NH_2OH, 99%, CAS No.: 5470–11–1, MilliporeSigma) solution for 5 min under shaking at 130 rpm by using an orbital shaker, followed by 25 min static incubation without shaking.

2.2. Nanoisland characterization

Scanning electron microscopy (SEM) images were obtained by a JSM-7600F Schottky field-emission scanning electron microscope (JEOL, Tokyo, Japan) at an accelerating voltage of 15.00 kV. The surface coverage and inter-island gap distance of gold nanoislands were determined from the SEM images by ImageJ software (National Institutes of Health, Bethesda, MD). Bulk refractive index sensitivity measurements were conducted by incubating the nanoisland platforms in water-glycerol mixtures with increasing glycerol fractions (0 to 40% v/v). Diced nanoisland platforms of 1 × 1 cm dimensions were placed into the wells of a 24-well plate by using double-sided tape. The optical extinction spectrum in each solution environment was recorded by using a microplate reader (SpectraMax iD5, Molecular Devices, San Jose, CA). For bulk refractive sensitivity analysis, the sensor response (R) was plotted as a function of the change in refractive index of the bulk solution and the slope of each plot was calculated by linear regression analysis. The corresponding general equation is $\Delta R/\Delta n$, where n is the refractive index of the medium. In our experiments, R was defined as the maximum-intensity wavelength in the optical extinction spectrum, λ_{max}, so the specific equation used in the analysis was $\Delta\lambda_{max}/\Delta n$ [32].

2.3. Protein detection measurements

A series of protein adsorption measurements was conducted to detect protein attachment to nanoisland platforms in terms of protein-substrate and protein-protein interactions. The measurements were conducted using a SpectraMax iD5 microplate reader and the optical extinction spectrum was recorded at each measurement step. In the first series, bovine serum albumin (BSA) protein (99%, CAS No.: 9048–46–8, MilliporeSigma) in Tris buffer (98%, CAS No.: 6976–37–0MilliporeSigma) (10 mM, 150 mM NaCl, pH 7.5) was added to the nanoisland platform with increasing BSA concentration from 0.001 to 100 µM in 10-fold increments. In the second series, a 100 µL volume of 5 µg/mL of recombinant COVID-19 nucleocapsid (N) protein antigen (catalog no. LIC-NP-04, LUCA AICell Inc., Anyang, Republic of Korea) in 50 mM carbonate coating buffer (pH 9.6) was added to the nanoisland platform and incubated at 37 °C for 1 h, as previously described [33]. Then, after washing three times with phosphate-buffered saline with 0.05% Tween 20 (CAS No.: 9005–64–5, MilliporeSigma) (PBS-T), a 100 µL volume of an anti-N, monoclonal primary antibody (clone 12D12, LUCA AI Cell Inc.) in PBS-T was added to the wells and incubated at 37 °C for 1 h. This step was followed by washing three times with PBS-T and then adding goat antihuman IgG secondary antibody (1:20,000 dilution; catalog no. A18811, Thermo Fisher Scientific, Waltham, MA) in PBS-T, which was incubated at 37 °C for 1 h, and another three rounds of washing with PBS-T. The optical extinction spectrum after each protein addition step was recorded by using a microplate reader (SpectraMax iD5).

3. Results and discussion

Fig. 1 presents the fabrication strategy to produce gold nanoislands on a glass substrate by using a thiol-based surface functionalization method. Compared to conventional nanoisland fabrication strategies based on solution-phase seeding, our strategy is based on the novel interplay of two ingredients: (1) the use of a thiol-functionalized glass surface to promote strong Au seed attachment to the substrate; and (2) the use of multiple growth cycles as com-

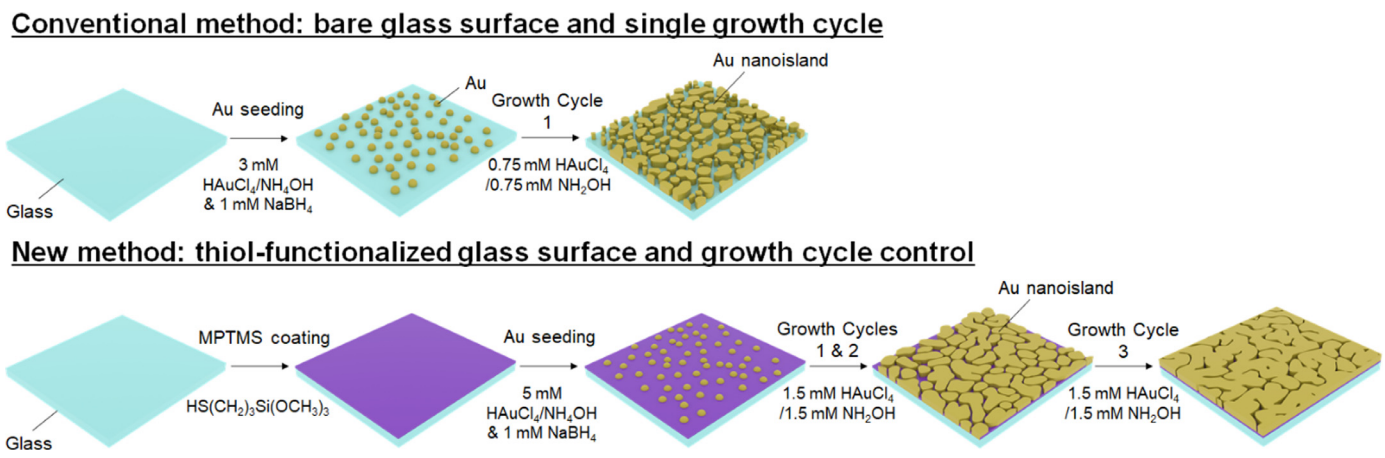

Fig. 1. Schematic illustration of the gold nanoisland fabrication process. The new method involves thiol-based surface functionalization of a glass surface, followed by solution-phase Au seeding and multiple nanoisland growth cycles thereafter. Controlling the number of growth cycles helps to finetune nanoisland features. By contrast, the conventional method involves a bare glass surface, solution-phase Au seeding, and a single growth cycle.

pared to only one cycle conventionally, in order to finetune nanoisland morphology.

Briefly, after washing a bare glass substrate with deionized water and acetone for 5 min, oxygen plasma treatment was performed for 1 min. Next, the glass substrate was coated with (3-mercaptopropyl)trimethoxysilane (MPTMS) by vacuum evaporation, which generated a thiol-terminated glass surface to promote strong gold-thiol interactions in the subsequent step [34]. The functionalized glass substrate was then immersed in 5 mM $HAuCl_4$, which served as the seeding solution. The subsequent addition of ammonium hydroxide under stirring created gold nucleation sites on the surface, which was followed by incubating the substrate in 1 mM sodium borohydride for 1 min. To promote nanoisland growth, the substrate was next immersed in an equimolar mixture of 1.5 mM $HAuCl_4$ and 1.5 mM NH_2OH as a growth solution for 5 min under orbital shaking and then left for 25 min without shaking at room temperature. To control the morphological properties of the gold nanoislands, the latter step was repeated 2 or 3 times in total depending on the sample. The same protocol steps were also used to fabricate gold nanoislands on a non-functionalized glass substrate without MPTMS coating for direct comparison.

For each fabricated substrate, we analyzed the morphological properties by visual inspection, scanning electron microscopy (SEM), and atomic force microscopy (AFM). In general, the solution-based fabrication method yielded plasmonic gold chips with high uniformity. For example, after 2 growth cycles, the gold nanoislands exhibited purple and blue colors on non-functionalized and functionalized glass substrates, respectively (**Supplementary Fig. 1**). Closer inspection by SEM imaging revealed key differences in the nanostructure morphology depending on the number of growth cycles and surface functionalization method. For gold nanoislands on non-functionalized glass surfaces, there was a large variation in the size of individual gold nanoislands (~10–80 nm) after 2 growth cycles and they tended to exhibit discrete, particle-like morphologies (**Fig. 2A**). After 3 growth cycles, the gold nanoisland film exhibited a more characteristic morphology of inhomogenous nanostructures with a percolated network pattern (**Fig. 2B**). However, a rather variable gap distance between nanoislands was observed. In marked contrast, after 2 growth cycles, a percolated network of inhomogenous gold nanoislands was already formed on the MPTMS-functionalized glass surface and the nanoislands exhibited tighter spacing and smaller apparent gap sizes (**Fig. 2C**). A similar nanoisland morphology also occurred on the MPTMS-functionalized glass surface after 3 growth cycles while the nanoislands in that case tended to be larger and more contiguous (**Fig. 2D**). These findings were corroborated by AFM measurements, which indicated that the nanoislands on non-functionalized glass surfaces had greater size/height variations whereas the nanoislands on MPTMS-functionalized surfaces exhibited more uniform size/height properties and greater continuity (**Supplementary Fig. 2**).

From a comparative perspective, we also quantitatively evaluated the surface coverage of gold nanoislands on the bare and MPTMS-functionalized glass surfaces by analyzing the SEM images. After 2 growth cycles, the surface coverage of gold nanoislands on bare and functionalized glass surfaces was around 50.4 ± 3.0 and 80.2 ± 3.9%, respectively (**Fig. 2E**). After 3 growth cycles, the surface coverage of gold nanoislands on bare and functionalized glass surfaces increased to around 66.8 ± 1.2 and 83.8 ± 3.0%, respectively (**Fig. 2F**). We also measured the inter-island gap distance between nanoislands. After 2 growth cycles, the mean gap distance on bare and functionalized glass surfaces was around 19.4 ± 1.2 and 8.7 ± 0.4 nm, respectively (**Fig. 2G**). After 3 growth cycles, the mean gap distance on bare and functionalized glass surfaces decreased to around 16.8 ± 0.9 and 7.3 ± 0.3 nm, respectively (**Fig. 2H**). Hence, gold nanoisland fabrication on the MPTMS-functionalized glass surface tended to yield higher surface coverages and smaller gap distances while modulating the glass surface properties and number of growth cycles enabled control over the surface coverage from ~50–83% and the gap distance from ~6–18 nm [35].

In order to evaluate the plasmonic properties of the gold nanoisland platforms, we proceeded to characterize the bulk refractive index (RI) sensitivity of the fabricated platforms by measuring changes in the optical extinction spectra in a series of water-glycerol mixtures, which had different refractive index values. The bulk RI sensitivity is a widely used performance metric to evaluate the sensing performance of nanoplasmonic sensors and describes the magnitude of the sensor response with respect to the change in the bulk refractive index of the bulk solution contacting the active side of the sensor surface [32,36]. Specifically, the changing medium conditions influence the plasmon-enhanced electromagnetic field surrounding the gold nanoislands and cause changes in the specific location of spectral features (*e.g.*, peaks) in the optical extinction spectrum, which can be tracked as sensor responses [32]. In general, the nanoisland platforms exhibited one dip and one peak in the extinction spectra and the quantitative value of the peak position (λ_{max}) was obtained by the centroid method, which improves the signal-to-noise ratio and has high accuracy, and was tracked as the sensor response in our experiments [37]. After 2

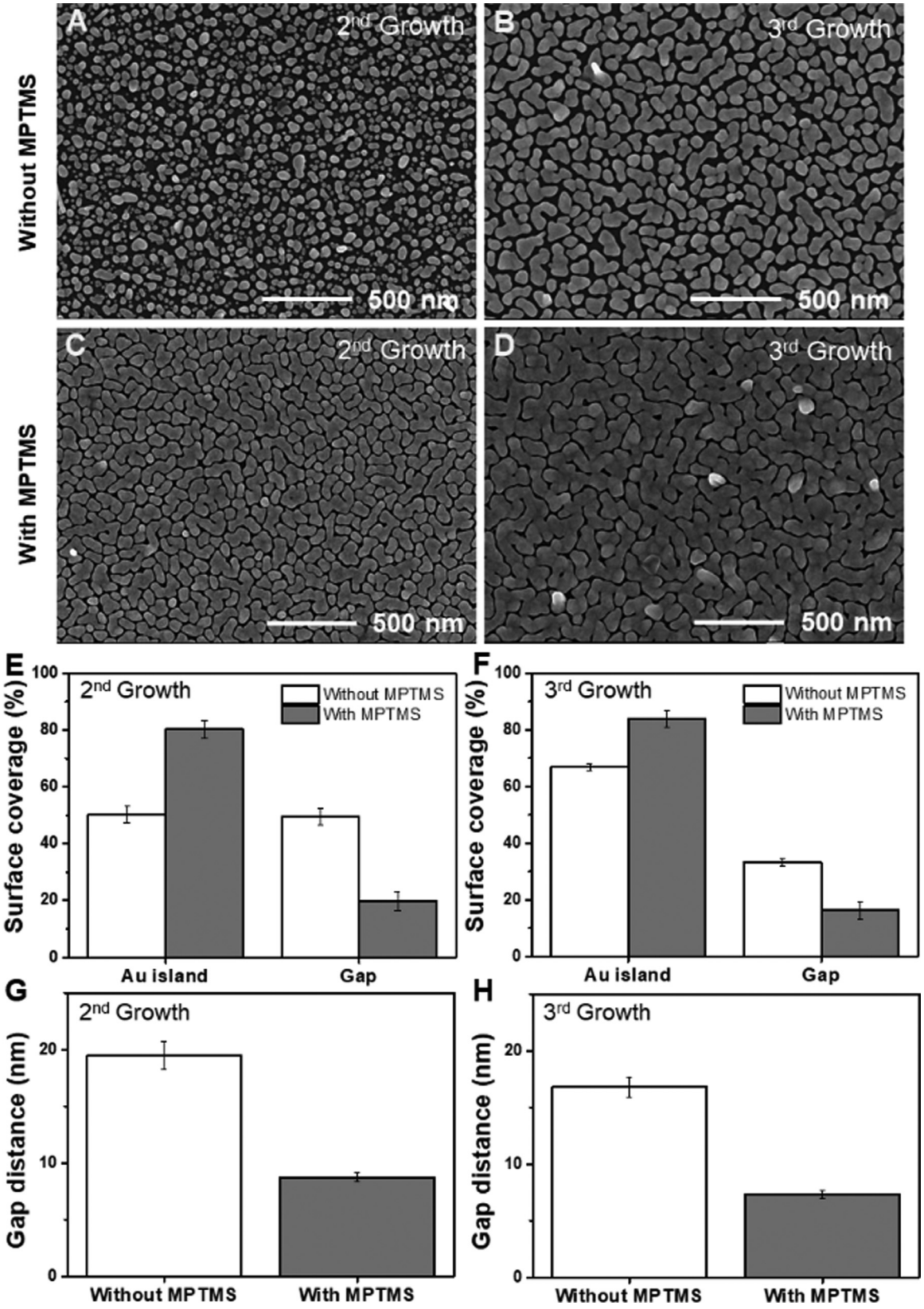

Fig. 2. Scanning electron microscopy (SEM) characterization of the gold nanoisland platform. Representative SEM images of gold nanoisland platforms fabricated on a bare glass surface after (A) 2 or (B) 3 growth cycles. Representative SEM images of gold nanoislands fabricated on an MPTMS-functionalized glass surface after (C) 2 or (D) 3 growth cycles. Corresponding surface coverage values of gold nanoislands and void spaces on bare and MPTMS-functionalized glass surfaces after (E) 2 or (F) 3 growth cycles. Corresponding inter-island gap distances for gold nanoislands on bare and MPTMS-functionalized glass surfaces after (G) 2 or (H) 3 growth cycles. For panels (E)–(H), data are reported as mean ± standard deviation.

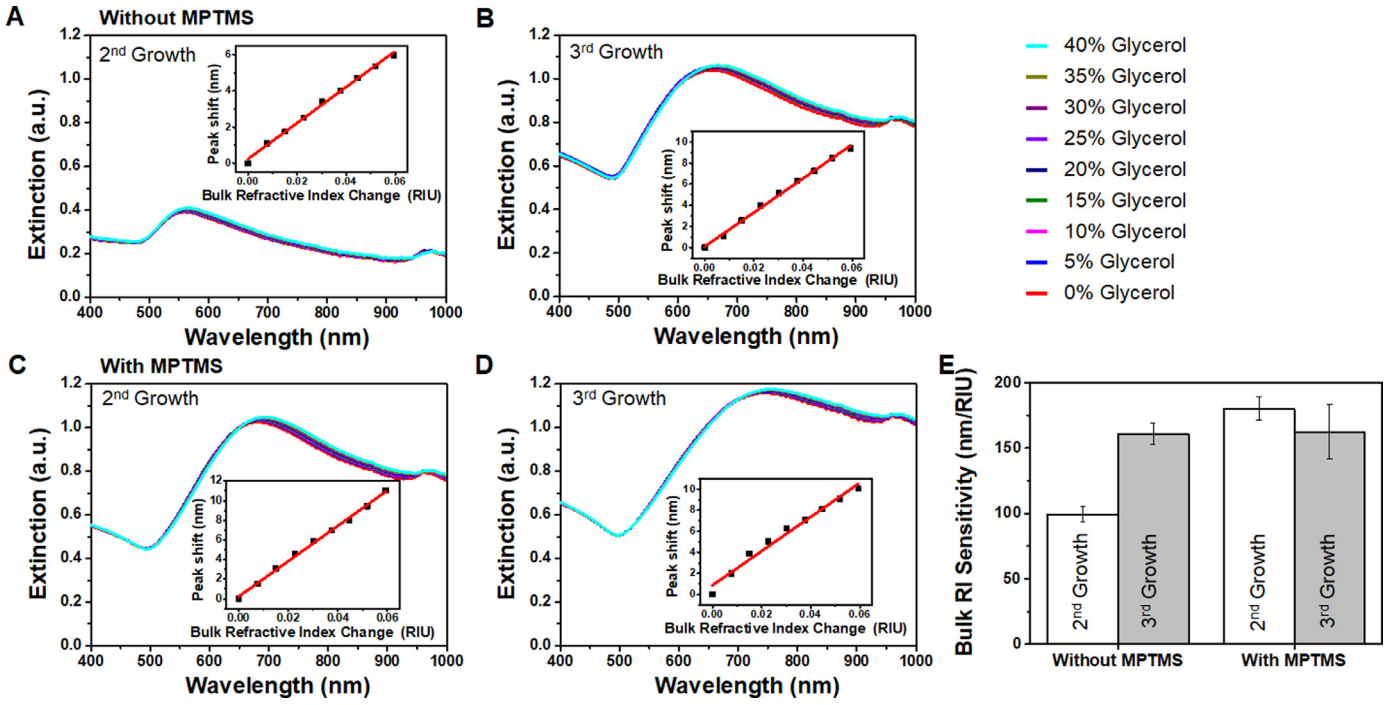

Fig. 3. Plasmonic characterization of gold nanoisland platforms. Optical extinction spectra of gold nanoislands on bare glass surfaces after (A) 2 or (B) 3 growth cycles and on MPTMS-functionalized glass surfaces after (C) 2 or (D) 3 growth cycles. Spectral shifts correspond to gold nanoislands in water-glycerol mixtures (0–40% v/v glycerol) with different refractive index values. Insets are linear fits of $\Delta\lambda_{max}$ shifts as a function of the refractive index change. (E) Summary of bulk refractive index values for the different nanoisland platforms. Data are reported as best-fit slope ± 95% confidence interval from the inset data in panels (A–D).

growth cycles, the nanoisland platform fabricated on the bare glass surface had relatively weak extinction intensity due to the low surface coverage and particle-like morphology, and the λ_{max} position in water was located at 559 nm (**Fig. 3A**). The corresponding bulk RI sensitivity value was 99.4 ± 5.8 nm per refractive index unit (nm/RIU) and the measurement response was linear. After 3 growth cycles, there was a higher extinction intensity and more characteristic spectral dip and peak features while the λ_{max} position in water increased to 660 nm and the bulk RI sensitivity value was 161.0 ± 8.2 nm/RIU with a linear response profile (**Fig. 3B**). On the other hand, even after 2 growth cycles, the nanoisland platform fabricated on the functionalized glass surface had clear spectral features, and the corresponding λ_{max} position in water was 679 nm while the bulk RI sensitivity value was 180.2 ± 8.9 nm/RIU and had a linear response profile (**Fig. 3C**). By contrast, after 3 growth cycles, the nanoisland platform fabricated on the functionalized glass surface had a less clear peak due to greater extinction on the long wavelength side of the spectrum (**Fig. 3D**). The corresponding λ_{max} position in water was 743 nm while the bulk RI sensitivity value had decreased to 162.5 ± 21.1 nm/RIU and had relatively less response linearity.

Together, these findings support that the nanoisland platform fabricated on the functionalized glass surface using 2 growth cycles, had the highest measurement sensitivity, which we selected for further protein detection testing (**Fig. 3E**). Importantly, these findings also support that optimizing the inter-island gap distance – rather than solely increasing or decreasing the gap distance – is important to maximize overlap of plasmon-enhanced electromagnetic waves for enhanced sensing performance, as indicated by the nonlinear trend between bulk RI sensitivity and gap distance whereby an intermediate gap distance corresponded to the highest sensitivity (**Supplementary Fig. 3**) [38]. Based on the SEM and AFM imaging results, we also estimated that the volumetric quantity of gold nanoislands per 1 μm^2 glass surface area was ~0.005 μm^3 and ~0.007 μm^3 on the non-functionalized and MPTMS-functionalized glass surfaces, respectively. The greater quantity of deposited gold on the MPTMS-functionalized glass surface is likely due to strong gold-thiol binding that facilitates high-density deposition of Au seeds and helps to overcome repulsive, inter-seed nanoparticle interactions, as compared to weaker attachment and in turn greater repulsive effects on the bare glass surface [35]. In turn, the higher seed density on the MTPMS-functionalized glass surface supports subsequent growth into more continuous, percolating nanostructures during subsequent growth cycles. The greater volumetric quantity of deposited gold may also partially relate to the improved sensing performance of the gold nanoisland platforms on the MPTMS-functionalized glass surface while the main contributing factor appears to be the nanoisland architecture and, more specifically, the inter-island gap distance.

To date, gold nanoisland platforms fabricated using solution-phase seeding strategies have been mainly utilized for SERS and plasmon-enhanced fluorescence detection applications, which motivated us to further explore their utility for refractometric biosensing applications. We first tracked bovine serum albumin (BSA) protein attachment onto the nanoisland platform by monitoring $\Delta\lambda_{max}$ shift changes in the optical extinction spectrum relative to baseline measurements in buffer only (**Fig. 4A**). The protein concentration was varied from 0.001 to 100 μM, which resulted in BSA concentration-dependent $\Delta\lambda_{max}$ shifts ranging from around 0.07 ± 0.04 nm to 8.93 ± 2.07 nm (**Fig. 4B**). To scrutinize protein-protein interactions, we also investigated the sequential attachment of coronavirus disease-2019 (COVID-19) nucleocapsid (N) protein antigen, primary antibody, and secondary antibody across three binding steps (**Fig. 4C**). The initial antigen attachment step yielded a $\Delta\lambda_{max}$ shift of around 3.0 ± 0.5 nm, while the final $\Delta\lambda_{max}$ shifts after primary and secondary antibody attachment were only marginally larger at 3.6 ± 0.4 and 3.8 ± 0.3 nm, respectively (**Fig. 4D**). These findings support that the gold nanoisland platform has a short decay length on the order of ~5–20 nm, which is consistent with the typical performance characteristics of

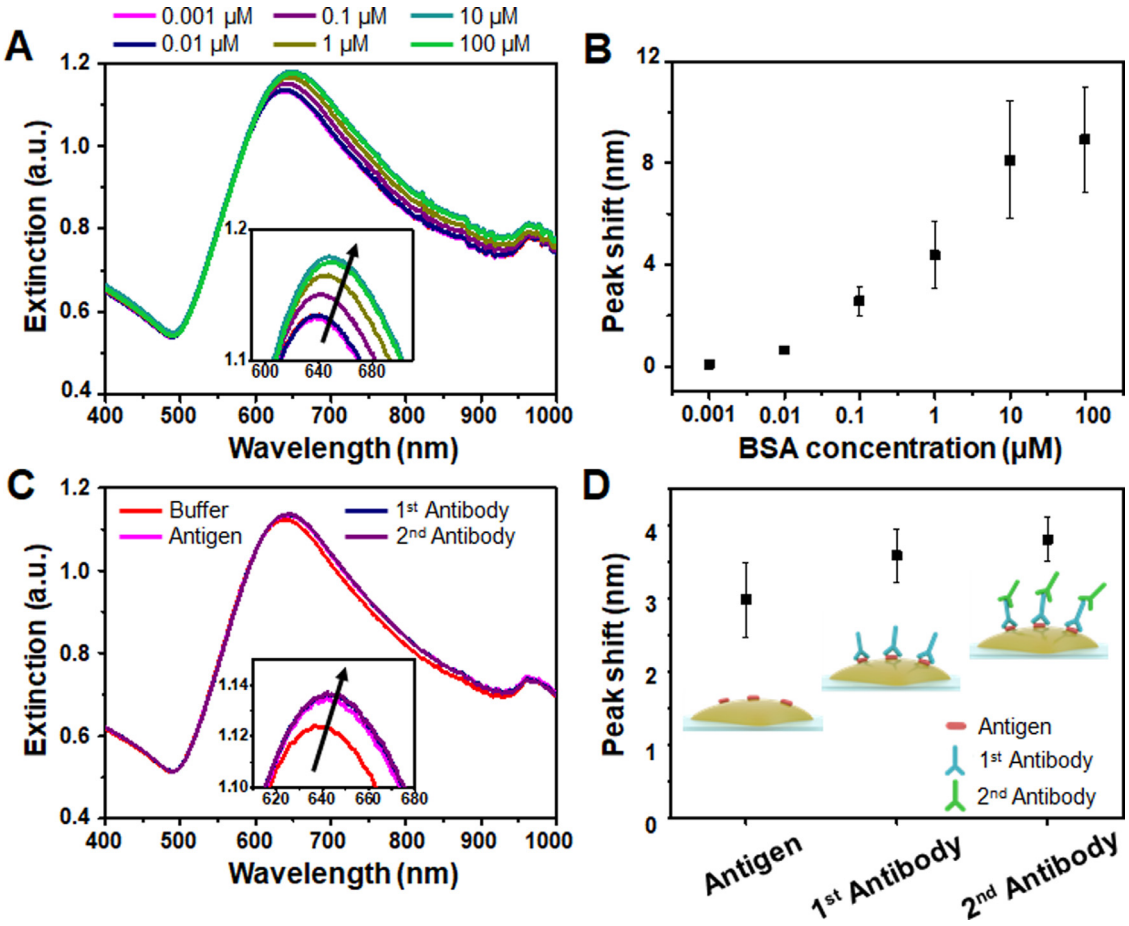

Fig. 4. Evaluation of gold nanoisland platform for protein detection. (A) Representative optical extinction spectra corresponding to 0.001–100 μM BSA protein addition to the gold nanoisland platform. Inset is a magnified view of the $\Delta\lambda_{max}$ shift region. (B) Final $\Delta\lambda_{max}$ shift values as a function of bulk BSA protein concentration corresponding to data in panel (A). (C) Representative optical extinction spectra corresponding to sequential addition of COVID-19 N protein antigen, anti-N primary antibody, and secondary antibody. Inset is a magnified view of the $\Delta\lambda_{max}$ shift region. (D) Final $\Delta\lambda_{max}$ shift values for different protein addition steps corresponding to data in panel (C). In panels (B) and (D), data are reported as mean ± standard deviation from $n = 3$ measurements.

Table 1
Biosensing performance comparison of the gold nanoisland platform developed in this study and other plasmonic nanostructures reported in the literature.

Type of substrate	BSA concentration (μM)	Bulk sensitivity (nm/RIU)	Peak shift (nm)	Refs.
Au nanoisland	100	180	8.9	Our work
Au nanohole	152	110	7	[41]
Au nanohole	15	247	1.6	[42]
Au nanodisk	100	100	0.7	[43]
Au nanoribbon	100	60	1	[44]
Au-coated nanograting	500	800	3.5	[45]
Au nanoparticle	50	642	7.4	[46]

surface-sensitive nanoplasmonic biosensors and demonstrates that the measurement response is highly sensitive to changes in the local refractive index near the sensor surface but less sensitive to changes occurring farther away from the sensor surface [39,40]. In terms of refractometric biosensing performance, it should also be noted that the $\Delta\lambda_{max}$ shift value of 8.9 nm is among the largest reported values for BSA protein attachment to a nanoplasmonic sensing platform that was directly fabricated on a substrate, further highlighting the highly surface-sensitive measurement capabilities of the gold nanoisland platform (**Table 1**).

4. Conclusions and outlook

In this study, we have developed a thiol-based surface functionalization strategy that improves gold nanoisland platform fabrication by increasing surface coverage of gold nanoislands and decreasing inter-island gap distance compared to nanoisland platforms fabricated on bare glass surfaces. The latter finding was particularly critical because we identified an optimal gap distance – within the range enabled by using thiol-functionalized glass surfaces but not achievable with conventional, bare glass surfaces using the same protocol steps – that facilitated superior nanoplasmonic sensing performance, as indicated by bulk RI sensitivity and response linearity. Importantly, this high measurement sensitivity translated into superior analytical capabilities for detecting protein attachment while additional experiments revealed that the gold nanoisland platform is particularly sensitive to detect adsorbing biomacromolecules that attach directly to the sensor surface as opposed to proteins involved in subsequent protein-protein interactions. Together, these findings demonstrate that the high sur-

face sensitivity of the gold nanoisland platform developed in this study can be useful for refractometric biosensing applications, especially in cases involving biomacromolecular interactions at the solid-liquid interfaces. While the main focus of the present study was on optimizing the gold nanoisland platform morphology to improve surface sensitivity, which was tested using purified natural proteins and recombinant antigens and antibodies, such platforms are regularly used for advanced biosensing applications involving complex media and can be readily functionalized using versatile surface chemistry options to facilitate measurement selectivity and sensitivity.

Data availability

The raw data required to reproduce these findings are available from the corresponding authors on reasonable request.

CRediT authorship contribution statement

Youngkyu Hwang: Conceptualization, Methodology, Investigation, Writing – original draft, Writing – review & editing. **Abdul Rahim Ferhan:** Investigation, Writing – review & editing. **Bo Kyeong Yoon:** Investigation, Resources, Writing – review & editing. **Tun Naw Sut:** Investigation, Resources, Writing – review & editing. **Won-Yong Jeon:** Investigation, Writing – review & editing. **Dong Jun Koo:** Investigation, Writing – review & editing. **Joshua A. Jackman:** Conceptualization, Methodology, Investigation, Writing – original draft, Writing – review & editing, Supervision. **Nam-Joon Cho:** Conceptualization, Methodology, Writing – review & editing, Supervision.

Declaration of Competing Interest

The authors declare no competing financial interest.

CRediT authorship contribution statement

Youngkyu Hwang: Conceptualization, Methodology, Investigation, Writing – original draft, Writing – review & editing. **Abdul Rahim Ferhan:** Investigation, Writing – review & editing. **Bo Kyeong Yoon:** Investigation, Resources, Writing – review & editing. **Tun Naw Sut:** Investigation, Resources, Writing – review & editing. **Won-Yong Jeon:** Investigation, Writing – review & editing. **Dong Jun Koo:** Investigation, Writing – review & editing. **Joshua A. Jackman:** Conceptualization, Methodology, Investigation, Writing – original draft, Writing – review & editing, Supervision. **Nam-Joon Cho:** Conceptualization, Methodology, Writing – review & editing, Supervision.

Acknowledgments

This work was supported by National Research Foundation of Korea (NRF) grants funded by the Korean government (MSIT) (2020R1C1C1004385 and 2020R1C1C1005523) and by the Basic Science Research Program through the National Research Foundation of Korea (NRF) funded by the Ministry of Education (2021R1I1A1A01056302). This work was also supported by the SKKU Research Fellowship Program of Sungkyunkwan University.

References

[1] J.B. Lassiter, M.W. Knight, N.A. Mirin, N.J. Halas, Reshaping the plasmonic properties of an individual nanoparticle, Nano Lett. 9 (2009) 4326–4332.
[2] Y. Jin, C. Jia, S.W. Huang, M. O'Donnell, X. Gao, Multifunctional nanoparticles as coupled contrast agents, Nat. Commun. 1 (2010) 41.
[3] I. Ruach-Nir, T.A. Bendikov, I. Doron-Mor, Z. Barkay, A. Vaskevich, I. Rubinstein, Silica-stabilized gold island films for transmission localized surface plasmon sensing, J. Am. Chem. Soc. 129 (2007) 84–92.
[4] S.M. Tabakman, Z. Chen, H.S. Casalongue, H. Wang, H. Dai, A new approach to solution-phase gold seeding for SERS substrates, Small 7 (2011) 499–505.
[5] M. Kuttge, F.J. Garcia de Abajo, A. Polman, Ultrasmall mode volume plasmonic nanodisk resonators, Nano Lett. 10 (2010) 1537–1541.
[6] Y. Liang, W. Cui, L. Li, Z. Yu, W. Peng, T. Xu, Large-scale plasmonic nanodisk structures for a high sensitivity biosensing platform fabricated by transfer nanoprinting, Adv. Opt. Mater. 7 (2019) 1801269.
[7] M.A. El-Sayed, Some interesting properties of metals confined in time and nanometer space of different shapes, Acc. Chem. Res. 34 (2001) 257–264.
[8] M.A. El-Sayed, Small is different: shape-, size-, and composition-dependent properties of some colloidal semiconductor nanocrystals, Acc. Chem. Res. 37 (2004) 326–333.
[9] C. Burda, X. Chen, R. Narayanan, M.A. El-Sayed, Chemistry and properties of nanocrystals of different shapes, Chem. Rev. 105 (2005) 1025–1102.
[10] A.R. Ferhan, Y. Hwang, M.S.B. Ibrahim, S. Anand, A. Kim, J.A. Jackman, N.J. Cho, Ultrahigh surface sensitivity of deposited gold nanorod arrays for nanoplasmonic biosensing, Appl. Mater. Today 23 (2021) 101046.
[11] T. Liu, J. Hsiung, S. Zhao, J. Kost, D. Sreedhar, C.V. Hanson, K. Olson, D. Keare, S.T. Chang, K.P. Bliden, P.A. Gurbel, U.S. Tantry, J. Roche, C. Press, J. Boggs, J.P. Rodriguez-Soto, J.G. Montoya, M. Tang, H. Dai, Quantification of antibody avidities and accurate detection of SARS-CoV-2 antibodies in serum and saliva on plasmonic substrates, Nat. Biomed. Eng. 4 (2020) 1188–1196.
[12] Z. Liang, Q. Zhang, Y. Nie, X. Zhang, Q. Ma, Polarized-electrochemiluminescence biosensor based on surface plasmon coupling strategy and fluorine-doped BN quantum dots, Anal. Chem. 92 (2020) 9223–9229.
[13] G. Qiu, Z. Gai, Y. Tao, J. Schmitt, G.A. Kullak-Ublick, J. Wang, Dual-functional plasmonic photothermal biosensors for highly accurate severe acute respiratory syndrome coronavirus 2 detection, ACS Nano 14 (2020) 5268–5277.
[14] A. Minopoli, B.D. Ventura, B. Lenyk, F. Gentile, J.A. Tanner, A. Offenhausser, D. Mayer, R. Velotta, Ultrasensitive antibody-aptamer plasmonic biosensor for malaria biomarker detection in whole blood, Nat. Commun. 11 (2020) 6134.
[15] J.B. Jackson, N.J. Halas, Surface-enhanced Raman scattering on tunable plasmonic nanoparticle substrates, Proc. Natl. Acad. Sci. U. S. A. 101 (2004) 17930–17935.
[16] F. De Angelis, F. Gentile, F. Mecarini, G. Das, M. Moretti, P. Candeloro, M.L. Coluccio, G. Cojoc, A. Accardo, C. Liberale, R.P. Zaccaria, G. Perozziello, L. Tirinato, A. Toma, G. Cuda, R. Cingolani, E. Di Fabrizio, Breaking the diffusion limit with super-hydrophobic delivery of molecules to plasmonic nanofocusing SERS structures, Nat. Photonics 5 (2011) 682–687.
[17] S. Krishnamoorthy, S. Krishnan, P. Thoniyot, H.Y. Low, Inherently reproducible fabrication of plasmonic nanoparticle arrays for SERS by combining nanoimprint and copolymer lithography, ACS Appl. Mater. Interfaces 3 (2011) 1033–1040.
[18] O. Graniel, I. Iatsunskyi, E. Coy, C. Humbert, G. Barbillon, T. Michel, D. Maurin, S. Balme, P. Miele, M. Bechelany, Au-covered hollow urchin-like ZnO nanostructures for surface-enhanced Raman scattering sensing, J. Mater. Chem. C 7 (2019) 15066–15073.
[19] G. Barbillon, O. Graniel, M. Bechelany, Assembled Au/ZnO nano-urchins for SERS sensing of the pesticide thiram, Nanomaterials 11 (2021) 2174.
[20] Y. Jeong, Y.M. Kook, K. Lee, W.G. Koh, Metal enhanced fluorescence (MEF) for biosensors: general approaches and a review of recent developments, Biosens. Bioelectron. 111 (2018) 102–116.
[21] S.M. Tabakman, L. Lau, J.T. Robinson, J. Price, S.P. Sherlock, H. Wang, B. Zhang, Z. Chen, S. Tangsombatvisit, J.A. Jarrell, P.J. Utz, H. Dai, Plasmonic substrates for multiplexed protein microarrays with femtomolar sensitivity and broad dynamic range, Nat. Commun. 2 (2011) 466.
[22] X. Li, T. Kuznetsova, N. Cauwenberghs, M. Wheeler, H. Maecker, J.C. Wu, F. Haddad, H. Dai, Autoantibody profiling on a plasmonic nano-gold chip for the early detection of hypertensive heart disease, Proc. Natl. Acad. Sci. U. S. A. 114 (2017) 7089–7094.
[23] V. Tvarožek, O. Szabó, I. Novotný, S. Kováčová, J. Škriniarová, P. Šutta, Plasmonic behaviour of sputtered Au nanoisland arrays, ApSS 395 (2017) 241–247.
[24] B. Miranda, K.Y. Chu, P.L. Maffettone, A.Q. Shen, R. Funari, Metal-enhanced fluorescence immunosensor based on plasmonic arrays of gold nanoislands on an etched glass substrate, ACS Appl. Nano Mater. 3 (2020) 10470–10478.
[25] M.A. Ibrahem, B.G. Rasheed, R.I. Mahdi, T.M. Khazal, M.M. Omar, M. O'Neill, Plasmonic-enhanced photocatalysis reactions using gold nanostructured films, RSC Adv. 10 (2020) 22324–22330.
[26] G. Gupta, D. Tanaka, Y. Ito, D. Shibata, M. Shimojo, K. Furuya, K. Mitsui, K. Kajikawa, Absorption spectroscopy of gold nanoisland films: optical and structural characterization, Nanotechnology 20 (2009) 025703.
[27] M.T. Do, Q.C. Tong, A. Lidiak, M.H. Luong, I. Ledoux-Rak, N.D. Lai, Nano-patterning of gold thin film by thermal annealing combined with laser interference techniques, Appl. Phys. A 122 (2016) 360.
[28] S. Badilescu, D. Raju, S. Bathini, M. Packirisamy, Gold nano-island platforms for localized surface plasmon resonance sensing: a short review, Molecules 25 (2020) 4661.
[29] B. Peng, G. Li, D. Li, S. Dodson, Q. Zhang, J. Zhang, Y.H. Lee, H.V. Demir, X.Y. Ling, Q. Xiong, Vertically aligned gold nanorod monolayer on arbitrary substrates: self-assembly and femtomolar detection of food contaminants, ACS Nano 7 (2013) 5993–6000.
[30] M.P. Cecchini, V.A. Turek, J. Paget, A.A. Kornyshev, J.B. Edel, Self-assembled nanoparticle arrays for multiphase trace analyte detection, Nat. Mater. 12 (2013) 165–171.

[31] K.R. Brown, L.A. Lyon, A.P. Fox, B.D. Reiss, M.J. Natan, Hydroxylamine seeding of colloidal Au nanoparticles. 3. controlled formation of conductive Au films, Chem. Mater. 12 (2000) 314–323.
[32] J.A. Jackman, A. Rahim Ferhan, N.J. Cho, Nanoplasmonic sensors for biointerfacial science, Chem. Soc. Rev. 46 (2017) 3615–3660.
[33] B.K. Yoon, T.N. Sut, K.Y. Yoo, S.H. Lee, Y. Hwang, J.A. Jackman, N.J. Cho, Lipid bilayer coatings for rapid enzyme-linked immunosorbent assay, Appl. Mater. Today 24 (2021) 101128.
[34] L. Supriya, R.O. Claus, Solution-based assembly of conductive gold film on flexible polymer substrates, Langmuir 20 (2004) 8870–8876.
[35] Y. Xue, X. Li, H. Li, W. Zhang, Quantifying thiol-gold interactions towards the efficient strength control, Nat. Commun. 5 (2014) 4348.
[36] J.A. Jackman, A.R. Ferhan, N.J. Cho, Surface-based nanoplasmonic sensors for biointerfacial science applications, Bull. Chem. Soc. Jpn. 92 (2019) 1404–1412.
[37] A.B. Dahlin, J.O. Tegenfeldt, F. Hook, Improving the instrumental resolution of sensors based on localized surface plasmon resonance, Anal. Chem. 78 (2006) 4416–4423.
[38] L.Y. Hsu, H.C. Yen, M.W. Lee, Y.L. Sheu, P.C. Chen, H. Dai, C.C. Chen, Large-scale inhomogeneous fluorescence plasmonic silver chips: origin and mechanism, Chem 6 (2020) 3396–3408.
[39] J. Li, J. Ye, C. Chen, Y. Li, N. Verellen, V.V. Moshchalkov, L. Lagae, P. Van Dorpe, Revisiting the surface sensitivity of nanoplasmonic biosensors, ACS Photonics 2 (2015) 425–431.
[40] F. Mazzotta, T.W. Johnson, A.B. Dahlin, J. Shaver, S.H. Oh, F. Höök, Influence of the evanescent field decay length on the sensitivity of plasmonic nanodisks and nanoholes, ACS Photonics 2 (2015) 256–262.
[41] D. Gao, W. Chen, A. Mulchandani, J.S. Schultz, Detection of tumor markers based on extinction spectra of visible light passing through gold nanoholes, Appl. Phys. Lett. 90 (2007) 073901.
[42] A. Hsiao, M.R. Gartia, T.W. Chang, X. Wang, P. Khumwan, G.L. Liu, Colorimetric plasmon resonance microfluidics on nanohole array sensors, Sens. Biosens. Res. 5 (2015) 24–32.
[43] J.A. Jackman, A.R. Ferhan, B.K. Yoon, J.H. Park, V.P. Zhdanov, N.J. Cho, Indirect nanoplasmonic sensing platform for monitoring temperature-dependent protein adsorption, Anal. Chem. 89 (2017) 12976–12983.
[44] C. Zhao, X. Xu, A.R. Ferhan, N. Chiang, J.A. Jackman, Q. Yang, W. Liu, A.M. Andrews, N.J. Cho, P.S. Weiss, Scalable fabrication of quasi-one-dimensional gold nanoribbons for plasmonic sensing, Nano Lett. 20 (2020) 1747–1754.
[45] S. Kumari, S. Mohapatra, R.S. Moirangthem, Development of flexible plasmonic plastic sensor using nanograting textured laminating film, Mater. Res. Express 4 (2017) 025008.
[46] S. Mariani, A. Paghi, A.A. La Mattina, A. Debrassi, L. Dahne, G. Barillaro, Decoration of porous silicon with gold nanoparticles via layer-by-layer nanoassembly for interferometric and hybrid photonic/plasmonic (bio)sensing, ACS Appl. Mater. Interfaces 11 (2019) 43731–43740.